

RESEARCH PAPER



LTN1 promotes RLR degradation to inhibit immune response to RNA virus through the ESCRT pathway

Fei Qin^{a,b*}, Baoshan Cai^{a,b*}, Peng Wang^c, Runyu Cao^{a,b}, Yuling Zhang^{a,b}, Hongling Wen^d, Yi Zheng^{a,b}, Wei Zhao^{a,e}, Chengjiang Gao^{a,b}, and Bingyu Liu^{a,b}

^aKey Laboratory of Infection and Immunity of Shandong Province & Key Laboratory for Experimental Teratology of Ministry of Education, Shandong University, Jinan, Shandong, China; ^bDepartment of Immunology, School of Basic Medical Sciences, Shandong University, Jinan, Shandong, China; ^cDepartment of Clinical Laboratory, The Second Hospital, Cheeloo College of Medicine, Shandong University, Jinan, Shandong, China; ^dDepartment of Microbiological Laboratory Technology, School of Public Health, Shandong University, Jinan, Shandong, China; ^eDepartment of Pathogenic Biology, School of Basic Medical Sciences, Shandong University, Jinan, Shandong, China

ABSTRACT

The excessive activation of immune responses will trigger autoimmune diseases or inflammatory injury. The endosomal sorting complexes required for transport (ESCRT) system can capture and mediate ubiquitinated protein degradation, which timely terminates signaling pathway hyperactivation. However, whether the ESCRT system participates in regulating RIGI-like receptor (RLR)-mediated antiviral responses remains unknown. In this study, we show that LTN1/listerin, a major component of RQC, can recruit E3 ubiquitin ligase TRIM27 to trigger K63-linked polyubiquitination of RIGI and IFIH1/MDA5. This K63-linked polyubiquitination facilitates the sorting and degradation of RIGI and IFIH1 proteins through the ESCRT-dependent pathway. Concordantly, LTN1 deficiency enhances the innate antiviral response to infection with RNA viruses. Thus, our work uncovers a new mechanism for RIGI and IFIH1 degradation and identifies the role of LTN1 in negatively regulating RLR-mediated antiviral innate immunity, which may provide new targets for the intervention of viral infection.

Abbreviation: 5'-pppRNA: 5' triphosphate double stranded RNA; ATG5: autophagy related 5; ATG7: autophagy related 7; BafA1: bafilomycin A₁; ESCRT: endosomal sorting complexes required for transport; CHX: cycloheximide; IFIH1/MDA5: interferon induced with helicase C domain 1; IFN: interferon; PIK3C3/VPS34: phosphatidylinositol 3-kinase catalytic subunit type 3; RIGI: RNA sensor RIG-I; RLR: RIGI-like receptors; RQC: ribosome-associated protein quality control; SeV: Sendai virus; TRIM27: tripartite motif-containing 27; VSV: vesicular stomatitis virus; VPS4: vacuolar protein sorting 4.

ARTICLE HISTORY

Received 14 April 2023
Revised 20 November 2023
Accepted 30 November 2023

KEYWORDS

Antiviral innate immunity;
ESCRT; LTN1; RLR;
ubiquitination





Introduction

Viral infectious diseases seriously endanger human survival and health, especially RNA viruses such as influenza virus and SARS-CoV-2 that have triggered epidemics in recent years [1,2]. The recent coronavirus disease 2019 (COVID-19) caused by SARS-CoV-2 has posed a great threat to human life and health. The virus is contagious, highly lethal, involves multiple organ system damage, causes a potentially fatal systemic disease, and has no specific drug, posing a challenge to countless countries and organizations around the world [3,4]. More than 770 million cases and 6.9 million deaths have been reported associated with COVID-19 (Available from: <https://covid19.who.int/>). Therefore, it is urgent to more comprehensively reveal how the host immune system fights viral infections and to develop key strategies to combat them.


Host immune surveillance systems detect viral nucleic acids by pattern recognition receptors (PRRs) [5]. RIGI (RNA sensor RIG-I)-like receptors (RLRs) are cytoplasmic RNA helicases that are responsible for the rapid recognition of virus RNA [6]. Specifically, after recognizing viral-derived RNA in the

cytoplasm, RIGI and IFIH1 then interact with the crucial adaptor MAVS (mitochondrial antiviral signaling protein) to transmit viral signals. MAVS then rapidly forms prion-like aggregates mediates on mitochondria to trigger the activation of the downstream effectors TBK1 (TANK-binding kinase 1) and IRF3 (interferon regulatory factor 3) which further induces the production of type I interferons (IFNs) and interferon-stimulated genes (ISGs) [7]. The IFNs responses are critical to innate antiviral immunity [8]. However, inappropriate immune reactions will contribute to immune-related tissue injury or autoimmune diseases [9]. Therefore, strict regulation of RLR signaling is essential to ensure successful virus elimination without detrimental immunopathology.

The endosomal sorting complexes required for transport (ESCRT) system, required for transport, captures ubiquitinated proteins and sequesters them into intraluminal vesicles in late endosomes. These vesicles mature into multivesicular bodies/MVBs, which eventually fuse with lysosomes for protein degradation [10]. The ESCRT pathway comprises five key complexes: ESCRT-0, ESCRT-I, ESCRT-II, ESCRT-III

CONTACT Chengjiang Gao  cgao@sdu.edu.cn  Key Laboratory of Infection and Immunity of Shandong Province & Department of Immunology, School of Biomedical Sciences, Shandong University, Jinan 250012, China; Bingyu Liu  liubingyu@sdu.edu.cn  Key Laboratory of Infection and Immunity of Shandong Province & Key Laboratory for Experimental Teratology of Ministry of Education, Shandong University, Jinan, Shandong 250012, China

*These authors contributed equally to this work.

 Supplemental data for this article can be accessed online at <https://doi.org/10.1080/15548627.2023.2291939>

complexes, and VPS4 (vacuolar protein sorting 4) [11]. ESCRT-0 [12], -I [13] and -II [14] complexes interact with proteins tagged with ubiquitin, clustering them in a specific membrane domain that undergoes invagination to form a luminal vesicle. Meanwhile, ESCRT-III forms the helical structure to seclude cargos, facilitating the curvature of the membrane toward the lumen [15]. Finally, ESCRT-III and VPS4 modify and split the membrane, recycling into the cytoplasm [16]. Two recent studies reported that ubiquitinated STING1 (stimulator of interferon response cGAMP interactor 1) can be trafficked to the endosome for degradation in an ESCRT-dependent mechanism [17,18], which suggests that the ESCRT complex could potentially regulate the innate antiviral signaling. However, the involvement of ESCRT systems in the degradation of RLRs is currently unknown.

Hijacking the host protein synthesis machinery to achieve large-scale virus production is one of the most common characteristics of viral infection. This process increases the probability of host ribosome stagnation and collision, leading to an imbalance of host protein synthesis homeostasis and triggering the activation of the ribosome-associated protein quality control (RQC) system [19]. The E3 ubiquitin ligase LTN1 (listerin E3 ubiquitin protein ligase 1) plays an important role in the RQC system. LTN1 binds to ribosomes and promotes the degradation of incomplete nascent polypeptides tagged with the ubiquitin through the proteasome pathway [20,21]. However, the role and mechanism of LTN1 in antiviral innate immunity are still unclear. In this study, we show that LTN1 can recruit E3 ubiquitin ligase TRIM27 to trigger K63-linked polyubiquitination of RIGI and IFIH1. This K63-linked polyubiquitination facilitates the sorting and degradation of RIGI and IFIH1 proteins through the ESCRT-dependent pathway. LTN1 deficiency promotes the innate antiviral response to infection with RNA viruses both *in vitro* and *in vivo*. Thus, our work uncovers a new mechanism for RIGI and IFIH1 degradation and a previously unknown function for LTN1 in negative regulation of antiviral innate immunity. This emphasizes the translational potential of targeting this pathway in virus invasion.

Results

LTN1 inhibits RLR-induced innate immune response

To investigate the role of LTN1 in innate immunity, we created the small interfering RNA (siRNA) to silence for the mouse *Ltn1* gene and performed the knockdown assays in peritoneal macrophages. mRNA and protein expression of LTN1 were efficiently knocked down, as measured by qPCR and western blotting analysis, respectively (Figure S1A). We then infected the macrophages with SeV or stimulated them with nucleic acid ligands, including the RNA mimics 5'-pppRNA and HMW poly(I:C). We observed that *Ifnb1* expression was upregulated in the LTN1-knockdown group compared to the control siRNA group upon SeV infection, as well as 5'-pppRNA or HMW poly(I:C) transfection (Figure S1B). The IFNB secretion induced by infection with SeV, as well as stimulation with 5'-pppRNA and HMW poly(I:C), was

also enhanced following the knockdown of LTN1 in macrophages (Figure S1C). We also transfected siRNA specific to human *LTN1* into THP-1 cells, a human monocyte cell line (Figure S1D). Knockdown of LTN1 in THP-1 cells significantly elevated *IFNB1* and *IFNA4* mRNA expression following infection with SeV or transfection with 5'-pppRNA (Figure S1E, F). We further explored the function of LTN1 in HEK293T cells with LTN1 overexpression, and found that overexpression of LTN1 decreased *IFNB1* mRNA after infection with SeV (Figure S1G). The immune response induced by SeV or EMCV infection or transfection of the RNA mimics 5'-pppRNA was predominantly initiated through the RLRs/MAVS pathway. Thus, our data suggest that LTN1 may negatively regulate antiviral innate immune responses mediated by RLRs.

To further verify the role of LTN1 in the regulation of IFNB production, we generated myeloid-specific *Ltn1*-deficient mice (*Ltn1^{fl/fl}Lyz2-Cre*) using the Cre/loxP technique. Mice with *Ltn1* loxP site was hybridized with *Lyz2-Cre* transgenic mice, in which exon 3–5 of *Ltn1* was specifically deleted by Cre recombinase expression on bone marrow cell-specific promoter *Lyz* (Figure 1A). We demonstrated that the protein level of LTN1 was obviously downregulated in peritoneal macrophages and bone marrow-derived macrophages (BMDMs) cultured from *Ltn1^{fl/fl}Lyz2-Cre* mice (Figure 1B). We then found that the *Ifnb1* and *Ifna4* mRNA levels were enhanced in *Ltn1*-deficient peritoneal macrophages than that in wild-type macrophages upon infection with SeV, as well as stimulation with 5'-pppRNA and infection with EMCV (Figure 1C–E). We further observed accordingly higher IFNB secretion in macrophages from *Ltn1^{fl/fl}Lyz2-Cre* mice than in those from wild-type mice (Figure 1F). The mRNA levels of *Ifnb1*, *Ifna4* and *Il6* were also increased in *Ltn1*-deficient BMDMs infected with SeV or stimulated with 5'-pppRNA and infected with EMCV (Figure S2A, B and C). We also established a *LTN1*-knockout HeLa cell line through the CRISPR-Cas9 system and found that knockout of *LTN1* in HeLa cells increased *IFNB1* production after SeV infection (Figure 1G).

IFNB plays a crucial role in innate antiviral immunity. Therefore, it was necessary to investigate the role of LTN1 in antiviral responses using the VSV virus. We prepared primary macrophages and transfected them with *LTN1* siRNA or control siRNA, followed by infection with VSV. Results showed that the siRNA knockdown of LTN1 expression increased VSV infection-induced *Ifnb1* mRNA levels. In contrast, the VSV replication was greatly decreased, as evidenced by lower viral mRNA levels and titers (Figure S3A). Similarly, the deficiency of LTN1 in THP-1 cells also promoted VSV infection-induced *IFNB1* expression, while VSV replication was decreased in the LTN1 knockdown group compared to the siRNA control group (Figure S3B). We further prepared peritoneal macrophages from *Ltn1^{fl/fl}* and *Ltn1^{fl/fl}Lyz2-Cre* mice followed by infection with VSV and we found that *LTN1* deficiency increased VSV infection-induced IFNB secretion, while attenuated VSV replication (Figure 1H,I). Overexpression of LTN1 in HEK293T cells resulted in decreased IFNB secretion and increased VSV mRNA and viral titer after

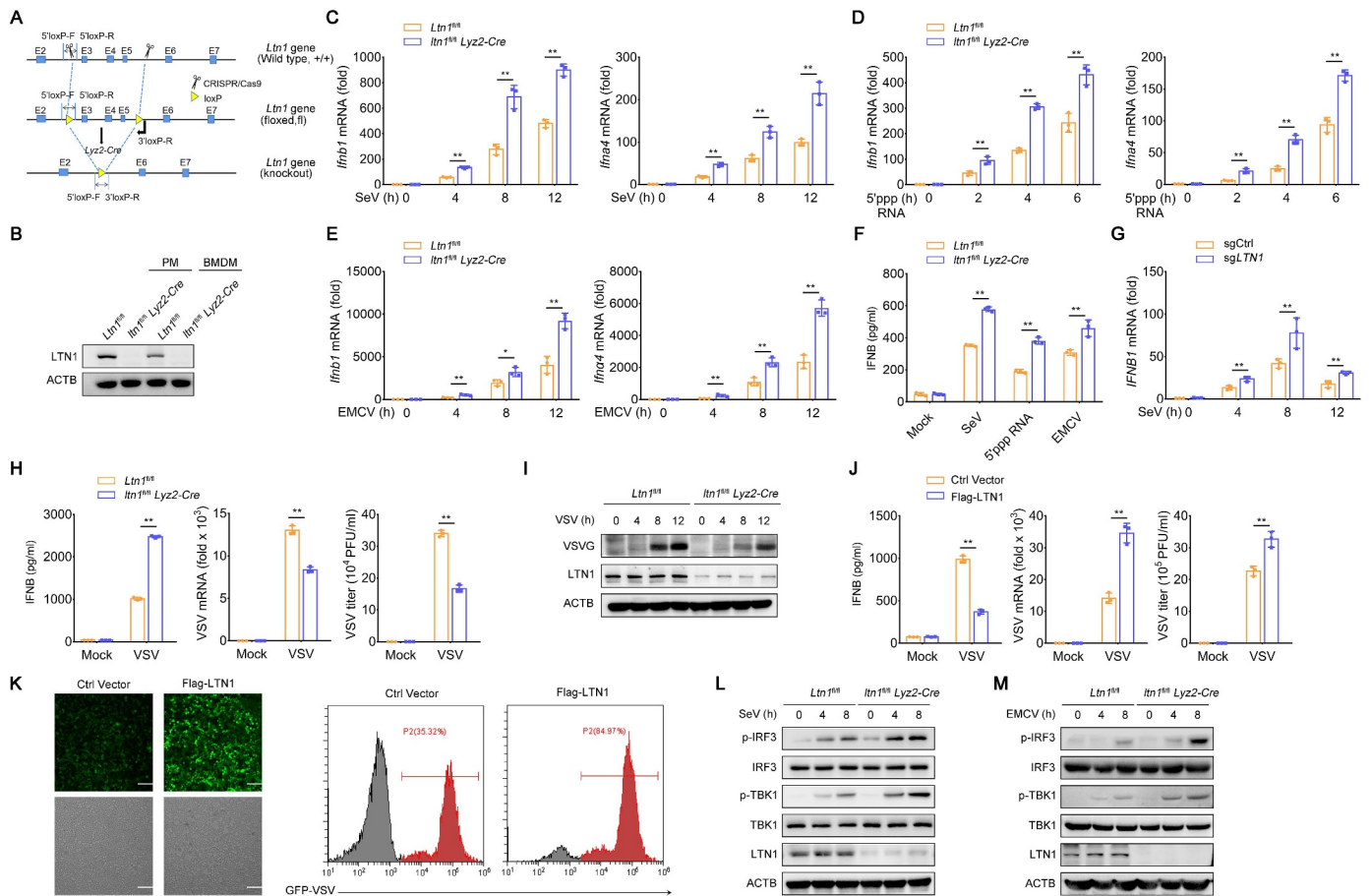


Figure 1. LTN1 negatively regulates cytosolic RNA-induced activation of innate immunity. (A) schematic description of myeloid lineage-specific *Ltn1*-knockout mice. (B) immunoblot analysis of LTN1 protein in peritoneal macrophages (PMs) and bone marrow derived macrophages (BMDMs). (C–E) qPCR analysis of *lfnb1*, *lfna4* mRNA in peritoneal macrophages from *Ltn1*^{fl/fl} and *Ltn1*^{fl/fl}*Lyz2-Cre* mice infected with SeV (C) or EMCV (E) for 0–12 h or transfected with 5'-pppRNA (D) for 0–6 h. (F) ELISA quantification of IFNB secretion in peritoneal macrophages from *Ltn1*^{fl/fl} and *Ltn1*^{fl/fl}*Lyz2-Cre* mice treated as in (C–E), mock, control (no stimulation). (G) qPCR analysis of *IFNB1* mRNA in wild-type HeLa cells (sgCtrl) and *LTN1*-knockout HeLa cells (sgLTN1) infected with SeV for 0–12 h. (H) secretion of IFNB measured by ELISA, VSV RNA measured by qPCR or VSV titers measured by plaque assay in *Ltn1*^{fl/fl} and *Ltn1*^{fl/fl}*Lyz2-Cre* peritoneal macrophages infected with VSV for 12 h. (I) immunoblot analysis of VSVG in *Ltn1*^{fl/fl} and *Ltn1*^{fl/fl}*Lyz2-Cre* peritoneal macrophages infected with VSV for 0–12 h. (J) Flag-LTN1 and control plasmid (Ctrl vector) were transfected in HEK293T cells followed by infection with VSV, secretion of IFNB, VSV RNA, VSV titers were determined. (K) HEK293T cells were transfected as in (J), VSV-GFP replication were determined by fluorescence microscopy (bright-field, upper; fluorescence, bottom). Scale bars: 100 μ m and flow cytometry analysis of the replication of GFP-VSV in HEK293T cells transfected as in (J) for 20 h, stimulated with VSV-GFP for 16 h, bars: 100 μ m. (L, M) immunoblot analysis of phosphorylated (*p*-) and total IRF3 and TBK1 in lysates of *Ltn1*^{fl/fl} and *Ltn1*^{fl/fl}*Lyz2-Cre* peritoneal macrophages infected with SeV (L) or EMCV (M) for 0, 4, 8 h. Data are from three independent experiments (C–H, J, mean \pm S.D. of triplicate assays) or are representative of three independent experiments with similar results. **P* < 0.05, ***P* < 0.01, Student's *t*-test.

infection with VSV virus (Figure 1J). Moreover, we used the GFP-VSV virus to infect HEK293T cells, and found increased levels of GFP-VSV in LTN1 overexpressing HEK293T cells (Figure 1K). These data indicate that LTN1 negatively regulates IFNB production triggered by RNA viruses, which facilitates the replication and escape of viruses.

To explore the role of LTN1 in RLR-mediated signaling, we detected that the phosphorylation of TBK1 and IRF3 was greater in macrophages from *ltn1*^{fl/fl}*Lyz2-Cre* mice than in macrophages from *Ltn1*^{fl/fl} mice after infection with SeV or EMCV (Figure 1L,M). Furthermore, the knocking out of LTN1 increased the phosphorylation of IRF3 and TBK1 in BMDMs from *ltn1*^{fl/fl}*Lyz2-Cre* mice than that from *Ltn1*^{fl/fl} mice after infection with SeV or EMCV (Figure S2D, E). Taken together, these data demonstrate that LTN1 negatively regulates RLRs-induced IFNB signaling to facilitate RNA virus infection.

LTN1 targets RIGI-IFIH1 and decreases their protein levels

To reveal the molecular mechanisms by which LTN1 inhibits RLR-mediated immunity, we first evaluated the effects of LTN1 on *IFNB1* expression in HEK293T cells mediated by key molecules in the RLR signaling pathway. We found that overexpression of Flag-LTN1 conspicuously decreased *IFNB1* mRNA expression in HEK293T cells transfected with RIG-IN or IFIH1, but not in cells transfected with MAVS, TBK1 or IRF3-5D (Figure 2A). These data indicate that LTN1 May target RIGI and IFIH1 in RLR signaling to regulate IFNB production and the antiviral response. Consistently, co-immunoprecipitation assays further showed that endogenous LTN1 formed complexes with RIGI or IFIH1 upon infection with SeV or EMCV in peritoneal macrophages (Figure 2B). Furthermore, confocal microscopy showed that LTN1 was co-localized with RIGI or IFIH1 (Figure 2C).

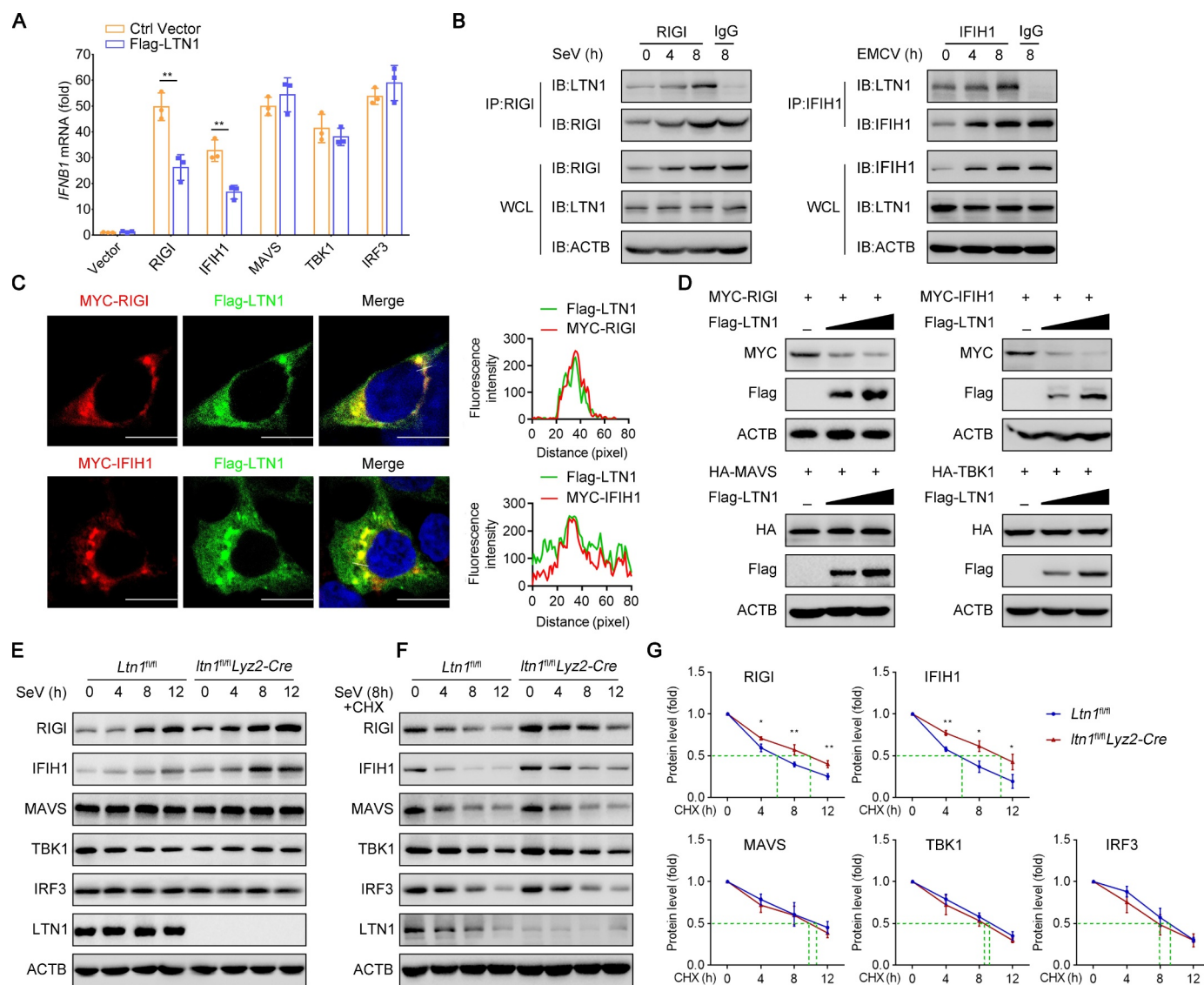


Figure 2. LTN1 targets RIGI-IFIH1 and decreases their protein levels. (A) qPCR analysis of *IFNB1* mRNA in HEK293T cells transfected for 24 h with control plasmid or plasmid expressing Flag-LTN1 together with expression plasmids for the RIGI N-terminal 2CARD (RIGIN), IFIH1, MAVS, TBK1, IRF3-5D (horizontal axes). (B) immunoprecipitation and immunoblot analysis of LTN1 and RIGI (left) infected with SeV or LTN1 and IFIH1 (right) infected with EMCV in mouse peritoneal macrophages for 0, 4, 8 h. (C) Flag- and MYC-specific immunostaining of HEK293T cells transfected with Flag-LTN1 and MYC-RIGI or MYC-IFIH1. Scale bars: 20 μ m. (D) MYC-RIGI, MYC-IFIH1, HA-MAVS, HA-TBK1 were transfected into HEK293T cells together with gradient amount of Flag-LTN1, the protein levels of RIGI or IFIH1 were detected by immunoblot. (E) immunoblot analysis of innate signaling proteins in *Ltn1^{fl/fl}* and *ltn1^{fl/fl}Lyz2-Cre* peritoneal macrophages infected with SeV for indicated times. (F) immunoblot analysis of innate signaling proteins in *Ltn1^{fl/fl}* and *ltn1^{fl/fl}Lyz2-Cre* peritoneal macrophages infected with SeV for 8 h, and then treated with the protein synthesis inhibitor CHX for the indicated times. (G) quantification analysis of proteins degradation kinetics in (F). Data are from three independent experiments (A, G, mean \pm S.D. of triplicate assays) or are representative of three independent experiments with similar results. * $P < 0.05$, ** $P < 0.01$, Student's *t*-test.

Considering the negative regulation of antiviral immunity by LTN1, we speculated that LTN1 may directly regulate the protein expression of RIGI or IFIH1. Therefore, we evaluated the expression of key molecules in the RLR signaling pathway upon LTN1 overexpression. MYC-RIGI, MYC-IFIH1, HA-MAVS and HA-TBK1 plasmids were co-transfected with Flag-LTN1 plasmid into HEK293T cells. We found the protein level of RIGI and IFIH1 was decreased in a dose-dependent manner by the exogenous expression of LTN1 (Figure 2D). In contrast, no such phenomenon was observed for the adaptor proteins MAVS or TBK1 (Figure 2D). Furthermore, we observed higher protein expression of RIGI and IFIH1 in the macrophages from *ltn1^{fl/fl}Lyz2-Cre* mice

after infection with SeV compared to macrophages from *Ltn1^{fl/fl}* mice (Figure 2E). While, the protein expression of MAVS, TBK1 and IRF3 was comparable between macrophages from *ltn1^{fl/fl}Lyz2-Cre* mice and macrophages from *Ltn1^{fl/fl}* mice (Figure 2E). Together, these data suggest that LTN1 interacts with RIGI and IFIH1 and affects their protein expression.

To investigate how LTN1 regulates RIGI and IFIH1 protein expression, peritoneal macrophages were first infected with SeV for 8 h, followed by treatment with the protein synthesis inhibitor cycloheximide (CHX) for different times. We then measured the protein degradation rate of various proteins in the RLR signaling pathway. We observed a delay

in the degradation of RIGI and IFIH1 proteins in *Ltn1*-deficient peritoneal macrophages. However, we found no differences in the degradation of MAVS, TBK1, or IRF3 proteins between macrophages from *ltn1^{fl/fl}Lyz2-Cre* mice and those from *Ltn1^{fl/fl}* mice (Figure 2F,G). Taken together, these results indicate that LTN1 May target RIGI and IFIH1 for degradation to regulate innate immunity.

LTN1 promotes the degradation of RIGI and IFIH1 through BECN1/PIK3C3 complex II independent of the conventional autophagy

To determine how LTN1 mediates the degradation of RIGI and IFIH1 proteins, we tested various inhibitors commonly used to study protein degradation. We found that LTN1-induced RIGI and IFIH1 degradation could be blocked by a specific vacuolar-type H⁺-translocating ATPase/V-ATPase inhibitor bafilomycin A₁ (BafA1) or autophagy inhibitors 3-methyladenine (3-MA) and wortmannin, but not by proteasome inhibitor MG132, indicating that LTN1 May promote RIGI and IFIH1 degradation through the autophagic processes (Figure 3A). BECN1 (beclin 1, autophagy related), ATG5 and ATG7 are core subunits regulating the autophagy pathway [22]. We then constructed *BECN1*, *ATG5*- and *ATG7*-knockout HEK293T cells using the CRISPR-Cas9 system. We found that LTN1-mediated degradation of RIGI and IFIH1 proteins was completely reversed in *BECN1*-knockout cells (Figure 3B). However, the degradation of RIGI and IFIH1 proteins remained unchanged after the knockout of *ATG5* and *ATG7* (Figure S4A, B). We investigated the role of selective autophagy and chaperone-mediated autophagy in LTN1-mediated degradation by using *SQSTM1/p62*- and *CALCOCO2/NDP52*-knockout cells, and LAMP2 knockdown cells. Despite the absence or downregulation of these proteins, LTN1 still promoted the degradation of RIGI and IFIH1 (Figure S4C, D and E).

BECN1 mainly forms two complexes in cells. Complex I is composed of the ATG14-BECN1-PIK3C3/VPS34-PIK3R4/VPS15, which is active on autophagosomes and participates in the nucleation process of autophagy. Complex II is composed of UVRAG-BECN1-PIK3C3-PIK3R4, which is mainly active in endocytic pathways through co-localizing with endolysosomal compartments [23]. PIK3C3 is the only class III phosphatidylinositol 3-kinase/PtdIns3K found in both complexes I and II. It phosphorylates phosphatidylinositol to produce phosphatidylinositol 3-phosphate, which regulates various biological processes, including cell growth and development, energy metabolism, and tumor progression. Our above data showed that phosphatidylinositol 3-kinase inhibitors 3-MA and wortmannin can block the LTN1-mediated degradation of RIGI and IFIH1. Thus, we speculate that PIK3C3 May participate in the LTN1-mediated degradation of the two receptors. To confirm this conclusion, we used CRISPR-Cas9 to knock out *PIK3C3* in HEK293T cells and found that the LTN1-mediated degradation of the two receptors were completely inhibited in the *PIK3C3*-knockout cells (Figure 3C). To further investigate the role of PIK3C3, we utilized SAR405, a specific inhibitor for PIK3C3. Consistent with the findings in Figure 3C, SAR405 blocked the

degradation of RIGI and IFIH1 proteins (Figure S4F). These data suggest that LTN1 promotes the degradation of RIGI and IFIH1 through BECN1-PIK3C3 complex II in an autophagy-independent manner.

LTN1 promotes the degradation of RIGI and IFIH1 through the ESCRT pathway

The BECN1-PIK3C3 complex II is active in the endocytic pathway through its co-localization with the endolysosomal compartment. Phosphatidylinositol 3-phosphate produced by PIK3C3 is enriched in early endosomes and can be identified by the HGS/HRS protein of ESCRT-0 in the ESCRT mechanism by anchoring the FYVE domain of ESCRT in the endosome. The ESCRT mechanism sorts ubiquitinated cargos within the endosomal chamber and packages them into vesicles that enter the endosomal lumen for eventual degradation. The ESCRT system consists of ESCRT-0, ESCRT-I, ESCRT-II, and ESCRT-III. ESCRT-0 includes HGS and STAM, which are crucial for sorting ubiquitinated cargos into endosomes. VPS4 remodels and cuts membranes, resulting in membrane tube formation and ultimately, membrane slicing. Thus, we next examined whether LTN1 promotes the degradation of RIGI and IFIH1 through the ESCRT system in endosomes by disturbing some key compartments of ESCRT.

To test the hypothesis, we used a siRNA mixture to simultaneously target *HGS*, *STAM*, and *STAM2* and disrupt the ESCRT-0 in HEK293T cells. Our findings indicate that LTN1-mediated degradation of RIGI and IFIH1 were abolished in HEK293T cells following siRNA knockdown of ESCRT-0 subunits (Figure S5A). We further constructed a *HGS*-knockout cell line and found that LTN1 completely lost its role in promoting the degradation of RIGI and IFIH1 in *HGS*-knockout HEK293T cells (Figure 3D). VPS4 is known to interact with ESCRT-III to promote the biogenesis of intraluminal vesicles and the formation of multivesicular endosomes, where ubiquitinated cargos are degraded. Consistently, we found that the LTN1-mediated degradation of RIGI and IFIH1 was similarly abolished in HEK293T cells following VPS4 siRNA knockdown (Figure S5B).

To obtain direct evidence for the internalization of RIGI and IFIH1 by LTN1 into acidic multivesicular bodies, we constructed an expression vector of GFP-mCherry-RIGI and -IFIH1, in which the green fluorescence of GFP quenches easily in an acidic environment, whereas the red fluorescence of mCherry is more stable. We transfected the vectors for GFP-mCherry-RIGI and -IFIH1 into HEK293T cells together with the LTN1 plasmid. Live cell time-lapse imaging showed a decrease in the green fluorescence of RIGI and IFIH1, as well as a slight decrease in the red fluorescence. In contrast, HEK293T cells transfected with control vector did not exhibit reduced green fluorescence, indicating that LTN1 specifically facilitates the internalization of RIGI and IFIH1 into acidic endosomes (Figure 3E). Importantly, the disappearance of GFP fluorescence was not observed in *HGS*-knockout cells (Figure 3F). Together, these data suggest that the ESCRT system is responsible for the degradation of RIGI and IFIH1 mediated by LTN1 in endosomes.

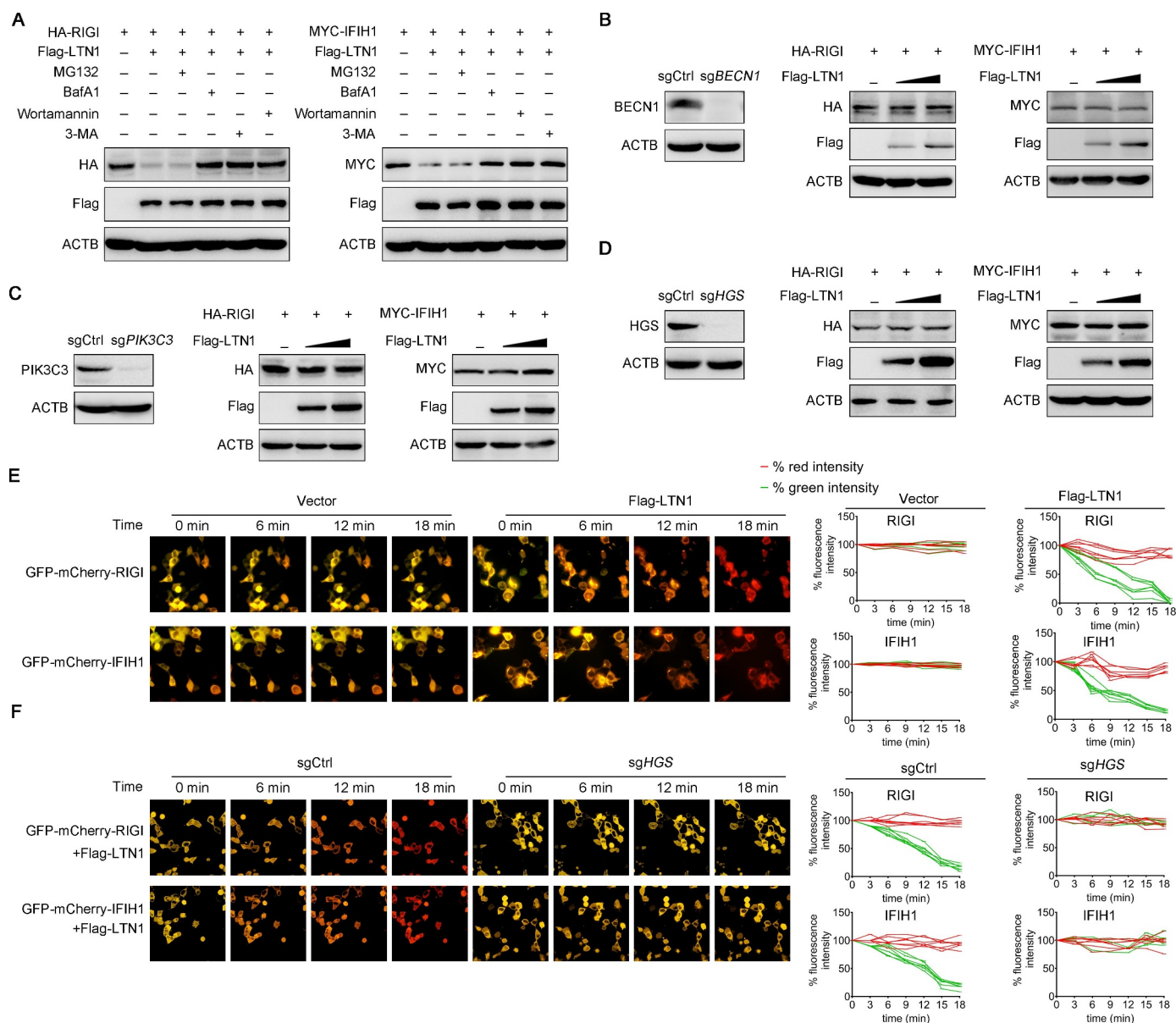


Figure 3. LTN1 promotes the degradation of RIGI and IFIH1 through BECN1-PIK3C3 complex II independent of conventional autophagy. (A) HA-RIGI or MYC-IFIH1 was transfected into HEK293T cells together with Flag-LTN1, followed by treatment with MG132 (10 μ M), BafA1 (0.5 μ M), wortmannin (10 μ M) or 3-methyladenine (10 mM) for 10 h. The protein levels of RIGI or IFIH1 were detected by immunoblot analysis. (B) HA-RIGI or MYC-IFIH1 was transfected into *BECN1*-knockout HEK293T cells (sg*BECN1*) together with gradient amount of Flag-LTN1, the protein levels of BECN1, RIGI or IFIH1 were detected by immunoblot analysis. (C) HA-RIGI or MYC-IFIH1 was transfected into *PIK3C3*-knockout HEK293T cells (sg*PIK3C3*) together with gradient amount of Flag-LTN1, the protein levels of PIK3C3, RIGI or IFIH1 were detected by immunoblot analysis. (D) HA-RIGI or MYC-IFIH1 was transfected into *HGS*-knockout HEK293T cells (sg*HGS*) together with gradient amount of Flag-LTN1, the protein levels of HGS, RIGI or IFIH1 were detected by immunoblot analysis. (E) GFP-mCherry-RIGI or GFP-mCherry-IFIH1 was transfected into HEK293T cells together with LTN1 plasmid or control plasmid. Representative confocal time lapse images every 6 min and quantitation of green and red fluorescence for RIGI and IFIH1 expression. (F) GFP-mCherry-RIGI or GFP-mCherry-IFIH1 was transfected into *HGS*-knockout HEK293T cells (sg*HGS*) or wild type HEK293T cells (sgCtrl) together with LTN1 plasmid. Representative confocal time lapse images every 6 min and quantitation of green and red fluorescence for RIGI and IFIH1 expression. Data are representative of three independent experiments with similar results.

LTN1 promotes K63-linked polyubiquitination on RIGI and IFIH1 independent of its E3 ligase activity

LTN1 is a RING-type E3 ubiquitin ligase involved in ubiquitination modification of aberrant nascent chains [24]. Cargos sorting into endosomes through ESCRT are predominantly tagged with lysine-63-linked polyubiquitin chains [25,26]. Thus, we investigated whether LTN1-mediated degradation of RIGI and IFIH1 occurs through protein ubiquitination. LTN1 contains a C-terminal RING domain (amino acids

1513–1762), a HEAT repeat-containing domain (amino acids 59–1512), and an N-terminal domain (amino acids 1–58). To investigate the functional domain that contributes to LTN1-mediated antiviral immunity, we generated several mutant plasmids including a point mutation LTN1 (C/A), in which the conserved cystines in the RING domain were mutated to alanines, a ring domain-deleted mutant LTN1 (Δ R), a HEAT domain, and a HEAT-lacking mutant (LTN1 [Δ HEAT]) (Figure 4A). We transfected these mutants into

HEK293T cells and measured *IFNB1* transcription after infection with SeV. We found that LTN1 mutants LTN1 (C/A) and LTN1 (Δ R) could still inhibit virus-infection induced *IFNB1* transcription. Conversely, the LTN1 mutant LTN1 (Δ HEAT) failed to attenuate infection-mediated *IFNB1* transcription (Figure 4B). Importantly, the LTN1 mutant with the HEAT domain alone was able to attenuate virus-induced *IFNB1* transcription (Figure 4B). Meanwhile, we showed that the HEAT domain of LTN1 was required for the LTN1-mediated degradation of RIGI and IFIH1 (Figure 4C).

To further investigate whether the E3 ligase activity of LTN1 was involved in this process, Flag-LTN1 (Δ R) was transfected into HEK293T cells together with MYC-RIGI or IFIH1 and HA-Ubiquitin plasmids. We found that the LTN1 (Δ R) could still increase the ubiquitination level of RIGI and IFIH1 (Figure 4D). Surprisingly, the overexpression of LTN1 (Δ HEAT) abolished the polyubiquitination of RIGI and IFIH1 (Figure 4E). These data demonstrate that LTN1 promotes the polyubiquitination of RIGI and IFIH1 independently of its E3 enzymatic activity. As polyubiquitin chains comprise several potential linkage residues, such as K6, K11, K27, K29, K33, K48, and K63, we investigated the type of polyubiquitin chains attached to RIGI and IFIH1 induced by LTN1. We found that LTN1 mainly promoted K63-linked ubiquitin chains in the presence of the inhibitor BafA1, but not other type ubiquitin chains to RIGI and IFIH1 (Figure 4F). To assess the ubiquitination of endogenous RIGI and IFIH1 induced by LTN1, we measured the polyubiquitination of RIGI and IFIH1 in primary macrophages prepared from *ltn1^{fl/fl}Lyz2-Cre* and *ltn1^{fl/fl}* mice with infection of SeV or EMCV. Our results showed that infection with SeV and EMCV increased both the K48- and K63-linked polyubiquitination of endogenous RIGI and IFIH1, respectively (Figure 4G). Notably, the K63-linked polyubiquitination of endogenous RIGI and IFIH1 was substantially decreased in *ltn1^{fl/fl}Lyz2-Cre* macrophages than in *ltn1^{fl/fl}* macrophages (Figure 4G).

Next, we reintroduced wild-type LTN1 or LTN1 (Δ HEAT) into LTN1-deficient HeLa cells. Reintroduction of wild-type LTN1 decreased *IFNB* transcription and IRF3 or TBK1 phosphorylation in LTN1-deficient HeLa cells (Figure 4H,I). Notably, reintroduction of LTN1 (Δ HEAT) in LTN1-deficient HeLa cells could not attenuate the SeV-induced expression of *IFNB1* or phosphorylation of IRF3 or TBK1 (Figure 4H,I). Consistent with the restoration of *IFNB1* transcription, the reintroduction of wild-type LTN1 in LTN1-deficient HeLa cells decreased the protein level of RIGI and IFIH1, whereas the reintroduction of LTN1 (Δ HEAT) had no such effect (Figure 4J). These results illustrate that the HEAT domain of LTN1 is indispensable for modulating the antiviral signaling pathway.

LTN1 enhances the K63-polyubiquitination of RIGI and IFIH1 by recruiting the E3 ubiquitin ligase TRIM27

As LTN1 enhanced the polyubiquitination of RIGI and IFIH1 independent of its enzymatic activity, we hypothesized that LTN1 might recruit other E3 ligase for K63-linked polyubiquitination. Through mass spectrometry analysis of LTN1-interacting proteins, we identified the E3 ubiquitin ligase TRIM27 as a potential candidate binding protein of LTN1 (Table S2). A previous related study has reported that

TRIM27 is localized on endosomes [27]. Therefore, we suspected that LTN1 likely recruits TRIM27 to facilitate the degradation of RIGI and IFIH1. The *in vitro* binding experiments with recombinant proteins revealed that RIGI and IFIH1 directly combine with LTN1 (Figure 5A). However, TRIM27 could not interact with RIGI and IFIH1 directly, the presence of LTN1 facilitated the interaction between TRIM27 and RIGI and IFIH1 (Figure 5A). To confirm LTN1 recruits TRIM27 to mediate the polyubiquitination of RIGI and IFIH1, we then performed the ubiquitination experiments *in vitro*. While LTN1 and TRIM27 together catalyzed the polyubiquitination of RIGI and IFIH1, indicating that LTN1 recruits the E3 ubiquitin ligase TRIM27 to promote RIGI and IFIH1 ubiquitination (Figure 5B). To confirm that TRIM27 is involved in LTN1-mediated degradation and polyubiquitination of RIGI and IFIH1, we used siRNA to knockdown TRIM27 expression. We found that TRIM27 siRNA knockdown could inhibit LTN1-mediated degradation and ubiquitination of RIGI and IFIH1 (Figure S6A, and S5C). To determine the role of TRIM27 in LTN1-mediated degradation and polyubiquitination of RIGI and IFIH1, we used CRISPR-Cas9 technology with a guide RNA specific to the human *TRIM27* gene (*sgTRIM27*) to establish *TRIM27*-knockout HEK293T cells. The mRNA levels of *Ifnb1* were increased in *TRIM27*-knockout HEK293T cells infected with SeV and EMCV (Figure S6B). Consistently, we also found that TRIM27 deficiency increased VSV infection-induced IFNB secretion, while attenuating VSV replication (Figure S6B). We also used the GFP-VSV virus to infect HEK293T cells, and found decreased levels of GFP-VSV in *TRIM27*-knockout HEK293T cells (Figure S6C). We further constructed the E3 ligase deficient mutant plasmid of TRIM27 (called “TRIM27 (C/A)” here), in which the two conserved catalytic cysteine residues within the TRIM27 RING domain (C16 and C31) were replaced with alanine [28,29]. Moreover, overexpression of WT His-TRIM27, but not the enzymatic mutant His-TRIM27 (C/A), rescued LTN1-mediated polyubiquitination of RIGI and IFIH1 in *TRIM27*-knockout HEK293T cells (Figure S6D). *In vitro* ubiquitination assay showed that TRIM27 could promote the polyubiquitination of RIGI and IFIH1 in the presence of LTN1, but not TRIM27 (C/A) (Figure S6E). Furthermore, *in vitro* binding assay also showed that the HEAT domain of LTN1, but not the RING domain also played a key role in recruiting TRIM27 and mediating interactions with RIGI, IFIH1, and TRIM27 (Figure S6F). Functionally, siRNA knockdown of TRIM27 prevented an increase in *Ifnb1* mRNA expression in *ltn1*-knockout macrophages infected with SeV (Figure 5D). Importantly, the disappearance of GFP fluorescence was not observed in *TRIM27*-knockout cells (Figure 5E), which suggested that TRIM27 was essential for LTN1-mediated degradation of RIGI and IFIH1. Overall, these results indicate that LTN1 recruits TRIM27 to promote the K63-linked polyubiquitination of RIGI and IFIH1, as well as subsequent degradation.

LTN1 negatively regulates anti-RNA viral responses *in vivo*

To investigate the significance of LTN1 in antiviral responses *in vivo*, *ltn1^{fl/fl}* and *ltn1^{fl/fl}Lyz2-Cre* mice were challenged

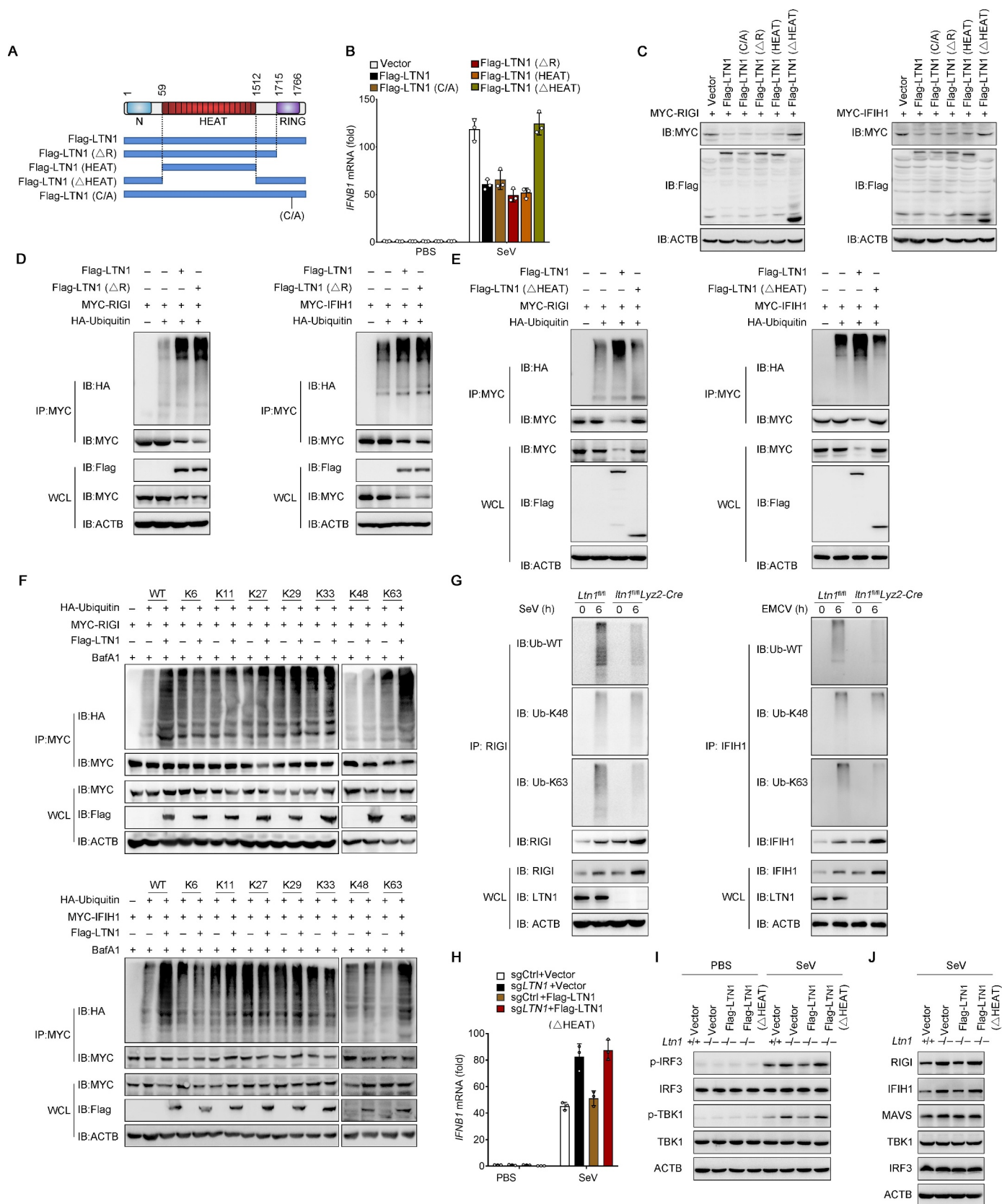


Figure 4. LTN1 promotes K63-linked polyubiquitination on RIGI and IFIH1 independent of its E3 ligase activity. (A) schematic structure of human LTN1 (WT) and its truncation mutants. (B) qPCR analysis of *IFNB1* mRNA in HEK293T cells transfected with expression plasmids for Flag-LTN1, Flag-LTN1 (C/A), Flag-LTN1 (ΔR), Flag-LTN1 (HEAT), and Flag-LTN1 (ΔHEAT) followed by infection with SeV for 8 h. (C) MYC-RIGI or MYC-IFIH1 was transfected into HEK293T cells together with plasmids for Flag-LTN1, Flag-LTN1 (ΔR), Flag-LTN1 (HEAT), and Flag-LTN1 (ΔHEAT), the levels of RIGI or IFIH1 were detected by immunoblot. (D) co-immunoprecipitation analysis of the ubiquitination of RIGI or IFIH1 in HEK293T cells transfected with plasmids encoding MYC-RIGI or MYC-IFIH1 and HA-Ubiquitin (WT), as well as a control vector or plasmids encoding Flag-LTN1, Flag-LTN1 (ΔR). (E) co-immunoprecipitation analysis of the ubiquitination of RIGI or IFIH1 in HEK293T cells transfected with plasmids encoding MYC-RIGI or MYC-IFIH1 together with HA-Ubiquitin and plasmids for Flag-LTN1 and Flag-LTN1 (ΔHEAT). (F) co-immunoprecipitation analysis of the ubiquitination of RIGI or IFIH1 in HEK293T cells co-transfected with MYC-RIGI or MYC-IFIH1 and HA-Ubiquitin (WT, K6, K11, K27, K29, K33, K48, K63) plasmids and

with VSV. We found that VSV-induced IFNB secretion was significantly increased in the serum from *ltn1^{fl/fl}Lyz2-Cre* mice compared to that from *Ltn1^{fl/fl}* mice (Figure 6A). In the spleen, liver, and lung of *ltn1^{fl/fl}Lyz2-Cre* mice infected with VSV, the expression of *Ifnb1* was higher than that of *Ltn1^{fl/fl}* mice (Figure 6B), which corresponded to a substantial reduction in VSV replication and titers (Figure 6C,D). Notably, severe pulmonary damage was observed in *Ltn1^{fl/fl}* mice following VSV infection (Figure 6E), while *ltn1^{fl/fl}Lyz2-Cre* mice showed a lower mortality risk compared to their matched controls (Figure 6F). These findings suggest that *Ltn1*-deficient mice are more resistant to RNA virus infection than wild-type mice.

Discussion

Viral infection may trigger translational stress, such as ribosome stalling or ribosome collision [30]. Colliding ribosomes can divide to produce 40S and 60S ribosomal subunits, which are recognized by ZNF598/HeI2 [31]. The 40S subunit is dissociated for recycling, while the 60S subunit still binds to the nascent peptidyl-tRNA conjugate [32]. Rqc2 is involved in identifying the 60S subunit and then recruiting the E3 ubiquitin ligase LTN1 for nascent peptide ubiquitination. The ubiquitinated peptide eventually enters the proteasome for degradation to alleviate ribosomal stress and ribosome rescue [31,33]. It has been reported that ASSC3 and ZNF598/HeI2, which are key molecules in the regulation of ribosome dissociation, play a role in the antiviral response by regulating innate immunity. The loss of ASSC3 function leads to increased ribosome collision, which can act as co-activators of CGAS [33]. The E3 ubiquitin ligase ZNF598/HeI2 can bind to RIGI, promote the non-covalent binding of FAT10 to RIGI, inhibit RIGI polyubiquitination, and negatively regulate RLR-mediated antiviral response [31]. All these indicate a significant correlation between viral infection and RQC response. However, as a key component of RQC, the function of LTN1 in the innate antiviral immune response is unclear. Our study found that LTN1 interacts with RIGI and IFIH1 on endosomes and promotes their K63-linked ubiquitination through recruitment of the E3 ligase TRIM27. Polyubiquitinated RIGI and IFIH1 are then recognized and sorted into endosomes by ESCRT machinery, leading to the degradation of these two receptors in endosomes (Figure 7).

The proper expression and activation of RIGI and IFIH1 are critical for inducing antiviral innate immune responses and promoting IFNB secretion [34]. However, unrestrained expression of RIGI and IFIH1 may lead to autoinflammatory and autoimmune diseases through the induction of RLR-induced signaling hyperactivation [35]. IFIH1 has been

discovered as a risk gene closely related to many autoimmune diseases. Genome-wide association studies indicated that IFIH1 gain-of-function mutants are closely related to type 1 diabetes (T1D) [36], systemic lupus erythematosus (SLE) [37], psoriasis [38] and Aicardi-Goutieres syndrome (AGS) [39]. Therefore, it is crucial to explore how to block RLR signaling to inhibit the overexpression of type I IFNs and prevent the occurrence of autoimmune diseases. Previous studies on the mechanism of RIGI and IFIH1 degradation mainly focused on the proteasome and classical autophagy pathways. Several E3 ubiquitin ligases, such as RNF125 [40], RNF122 [41] and TRIM40 [42], promoted RIGI or IFIH1 ubiquitin modification and proteasome pathway degradation. CCDC50 [43] and LRRC25 [44] delivered the over-activated RIGI-IFIH1 for autolysosomal degradation. However, ESCRT system regulates the protein expression of RIGI and IFIH1 has not been reported. Consequently, our study reveals an innovative degradation pathway for RIGI and IFIH1 mediated by LTN1 through the ESCRT-dependent pathway.

LTN1 comprises a conserved N-terminal domain, ARM and HEAT repeats, and a RING domain in the C-terminal. The N-terminal domain is required to interact with 60S subunits, and the RING domain provides E3 ligase activity required for the ubiquitination and degradation of nascent proteins [45]. However, the function of the ARM-HEAT repeats remains enigmatic, although they are assumed to solely represent the link between LTN1 ends and distal sites on the ribosome [20,21]. Unexpectedly, we found that the E3 ligase activity of LTN1 is not necessary for the degradation of RIGI and IFIH1, which differs from its function in the RQC-mediated degradation of aberrant nascent polypeptide. Interestingly, the HEAT domain is crucial in this process. Deletion of the HEAT domain impaired the effect of LTN1 during regulation of the innate immune response. Consistently, knockout of *NEMF* and *TCF25*, which encode another two components in the RQC system that facilitate the degradation of nascent protein by LTN1 (46), does not affect LTN1-induced degradation of RIGI and IFIH1 (Figure S7A, 7B). Therefore, we concluded that LTN1 can degrade these two key receptor proteins in the antiviral signaling pathway, regulating antiviral response independently of the RQC function.

Considering that the RING domain of LTN1 is dispensable for the degradation of RIGI and IFIH1, LTN1 may use other E3 ubiquitin ligases to promote the K63-linked ubiquitination of RIGI and IFIH1. Indeed, we found that LTN1 can recruit TRIM27 to mediate the ubiquitin modification of RIGI and IFIH1. Our study found that TRIM27 mediated the K63-linked ubiquitin modification of RIGI and IFIH1 for degradation in an ESCRT-dependent mechanism. Previous study has reported that TRIM27 can induce TBK1 degradation via K48-

Flag-LTN1 followed by treatment with BafA1. (G) *Ltn1^{fl/fl}* and *ltn1^{fl/fl}Lyz2-Cre* peritoneal macrophages were infected with SeV (left), EMCV (right) for 6 h, endogenous ubiquitination of RIGI or IFIH1 were assessed by immunoblot analysis with anti-ubiquitin, anti-K48 ubiquitin or anti-K63 ubiquitin after immunoprecipitation with anti-RIGI or anti-IFIH1 and by immunoblot analysis with input proteins and loading control. (H) qPCR analysis of *IFNB1* mRNA of wild type HeLa cells (sgCtrl) and *LTN1*-knockout HeLa cells (sg*LTN1*) transfected for 24 h with expression plasmids for Flag-LTN1, and Flag-LTN1 (Δ HEAT) followed by infection with SeV for 8 h. (I) immunoblot analysis of phosphorylated (*p*-) and total IRF3 and TBK1 in lysates of wild type HeLa cells (sgCtrl) and *LTN1*-knockout HeLa cells (sg*LTN1*) transfected as in (H) followed by infection with SeV for 8 h. (J) immunoblot analysis of innate signaling proteins in wild type HeLa cells (sgCtrl) and *LTN1*-knockout HeLa cells (sg*LTN1*) transfected as in (I) followed by infection with SeV for 8 h. Data are from three independent experiments (B, H, mean \pm S.D. of triplicate assays) or representative of three independent experiments with similar results.

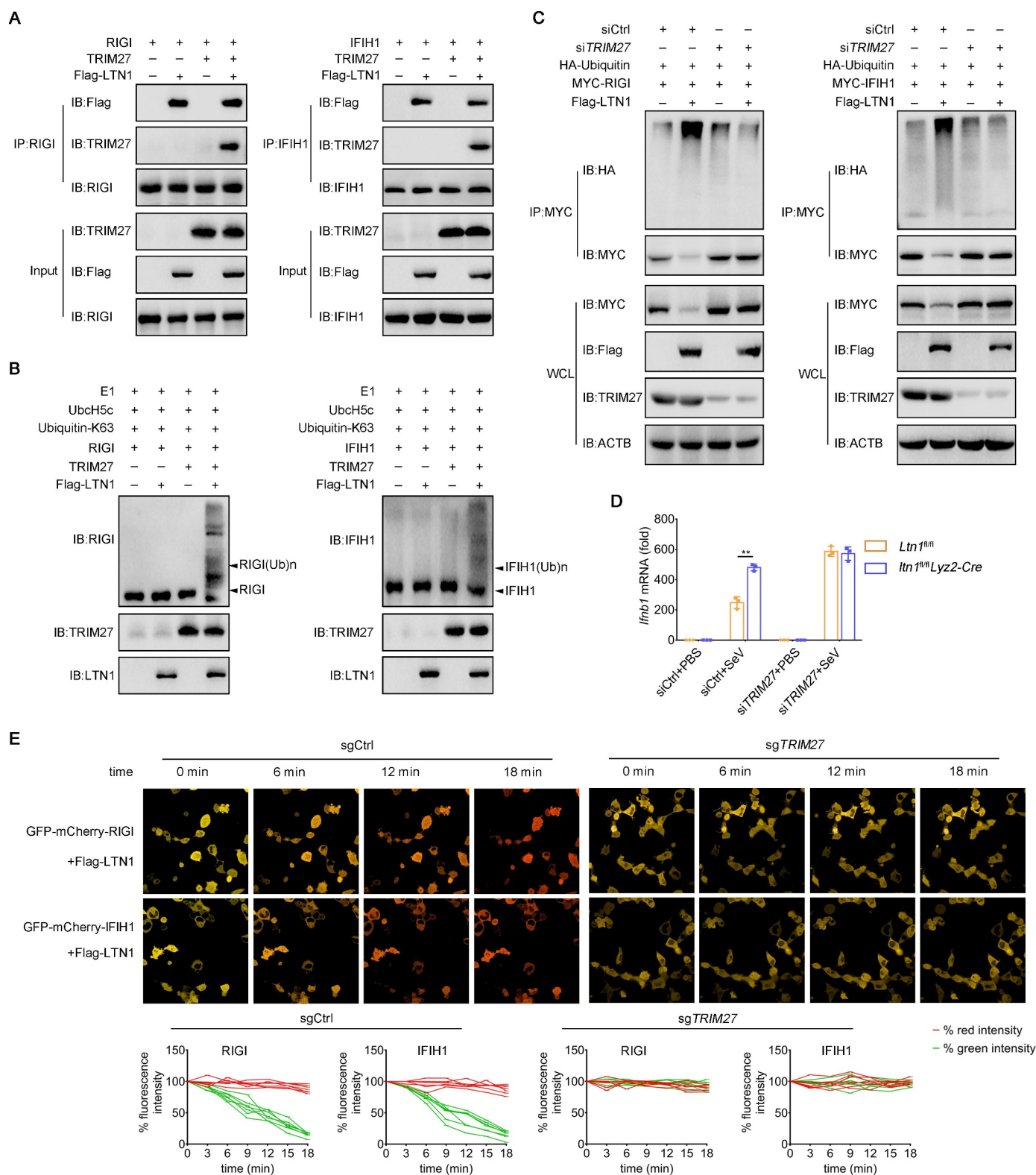


Figure 5. LTN1 enhances the K63-polyubiquitination of RIGI and IFIH1 by recruiting the E3 ubiquitin ligase TRIM27. (A) *in vitro* affinity-isolation assay of RIGI or IFIH1 with LTN1, TRIM27 using purified recombinant proteins. (B) *in vitro* ubiquitination assay of RIGI or IFIH1 in HEK293T cells transfected with *siTRIM27* and control siRNA for 24 h followed by transfection of the plasmids expressing MYC-RIGI or MYC-IFIH1, HA-Ubiquitin, and Flag-LTN1 or Flag control vector. (C) co-immunoprecipitation analysis of the ubiquitination of RIGI or IFIH1 in HEK293T cells transfected with *siTRIM27* and control siRNA for 24 h followed by transfection of the plasmids expressing MYC-RIGI or MYC-IFIH1, HA-Ubiquitin, and Flag-LTN1 or Flag control vector. (D) peritoneal macrophages from *Ltn1^{fl/fl}* and *Ltn1^{fl/fl}Lyz2-Cre* mice were transfected siRNA against TRIM27 and control siRNA, followed by infection with SeV for 8 h, the *lfnb1* mRNA levels were detected by qPCR analysis. (E) GFP-mCherry-RIGI or GFP-mCherry-IFIH1 was transfected into *TRIM27*-knockout HEK293T cells (sgTRIM27) or wild-type HEK293T cells (sgCtrl) together with LTN1 plasmid. Representative confocal time lapse images every 6 min and quantitation of green and red fluorescence for RIGI and IFIH1 expression. Data are from three independent experiments (D, mean \pm S.D. of triplicate assays) or are representative of three independent experiments with similar results. ** $P < 0.01$, Student's *t*-test.

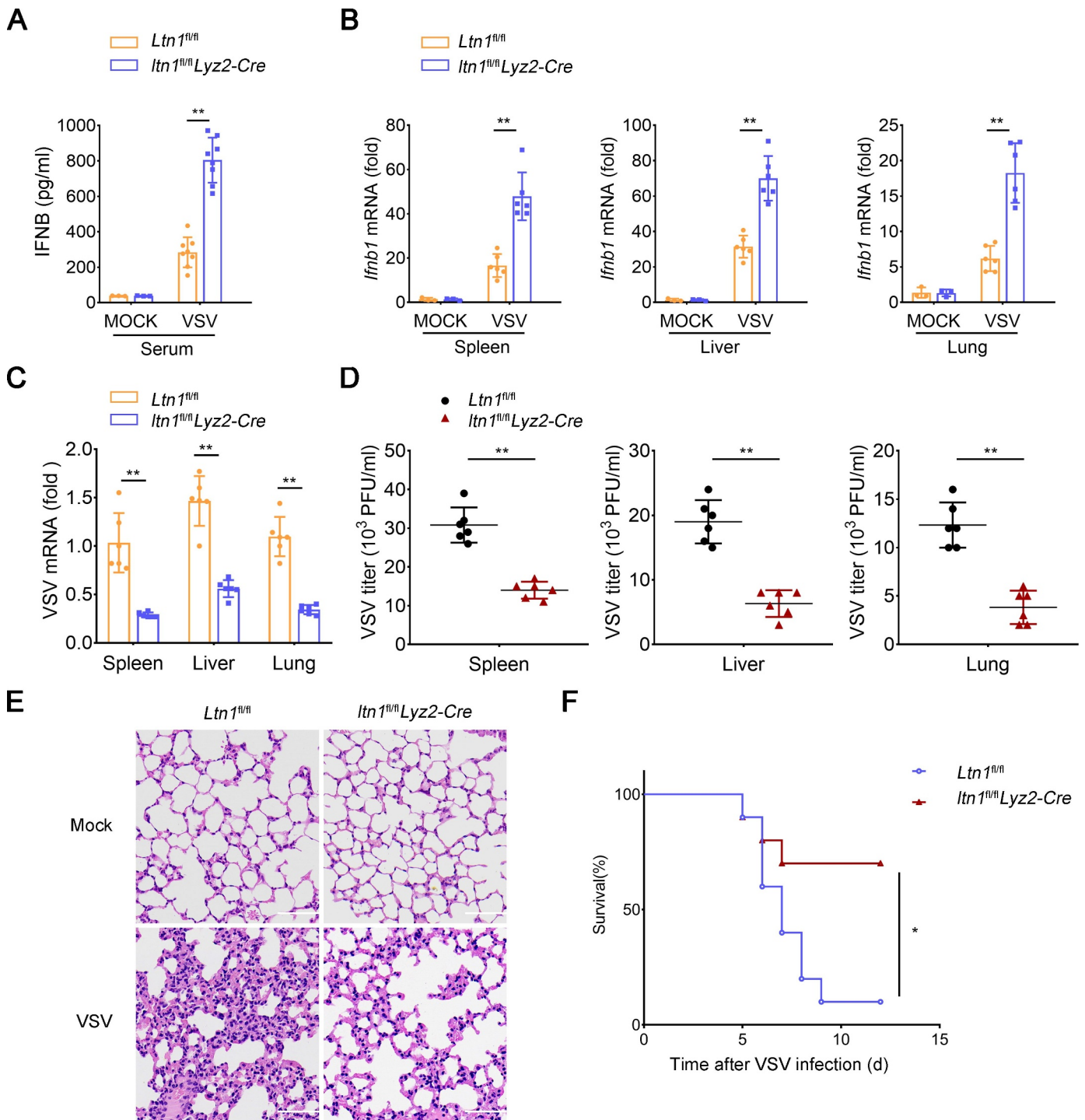


Figure 6. Deficiency of LTN1 enhances type I IFN production and protects mice from RNA viral infection. (A) IFN β secretion in sera from $Ltn1^{fl/fl}$ and $Ltn1^{fl/fl}Lyz2-Cre$ mice after intraperitoneal injection for 8 h with VSV (5×10^7 PFU per mouse). (B) expression of *Ifnb1* mRNA in the spleen (left), liver (middle) and lung (right) by qPCR analysis from $Ltn1^{fl/fl}$ and $Ltn1^{fl/fl}Lyz2-Cre$ mice ($n = 6$ /group) infected for 48 h by intraperitoneal injection of VSV for 48 h (5×10^7 PFU per mouse). (C) expression of VSV mRNA in the spleen, liver and lung by qPCR analysis from $Ltn1^{fl/fl}$ and $Ltn1^{fl/fl}Lyz2-Cre$ mice infected for 48 h by intraperitoneal injection of VSV (5×10^7 PFU per mouse). (D) plaque assay of viral titers in the spleen (left), liver (middle) and lung (right) from $Ltn1^{fl/fl}$ and $Ltn1^{fl/fl}Lyz2-Cre$ mice infected with the VSV for 48 h (5×10^7 PFU per mouse). (E) hematoxylin-and-eosin-stained images of lung sections of $Ltn1^{fl/fl}$ and $Ltn1^{fl/fl}Lyz2-Cre$ mice infected for 48 h by intraperitoneal injection of VSV (5×10^7 PFU per mouse); Scale bars: 100 μ m. (F) survival of $Ltn1^{fl/fl}$ and $Ltn1^{fl/fl}Lyz2-Cre$ mice after intravenous injection of VSV (1×10^8 PFU per mouse). Data are from three independent experiments (A-D, mean \pm S.D. of triplicate assays). * $P < 0.05$, *** $P < 0.01$, Student's *t*-test (A-D), the log-rank mantel-cox test (F).

linked ubiquitination to inhibit type I IFN production and suppress antiviral innate immune response [46]. This suggests that TRIM27 May potentially regulate antiviral innate immunity through multiple targets. Our study provides new insights

and a broader perspective that further sheds light on TRIM27's contribution to the antiviral immune process.

In summary, we identified LTN1 as a suppressor of anti-RNA viral innate immunity by targeting RIGI and IFIH1, in

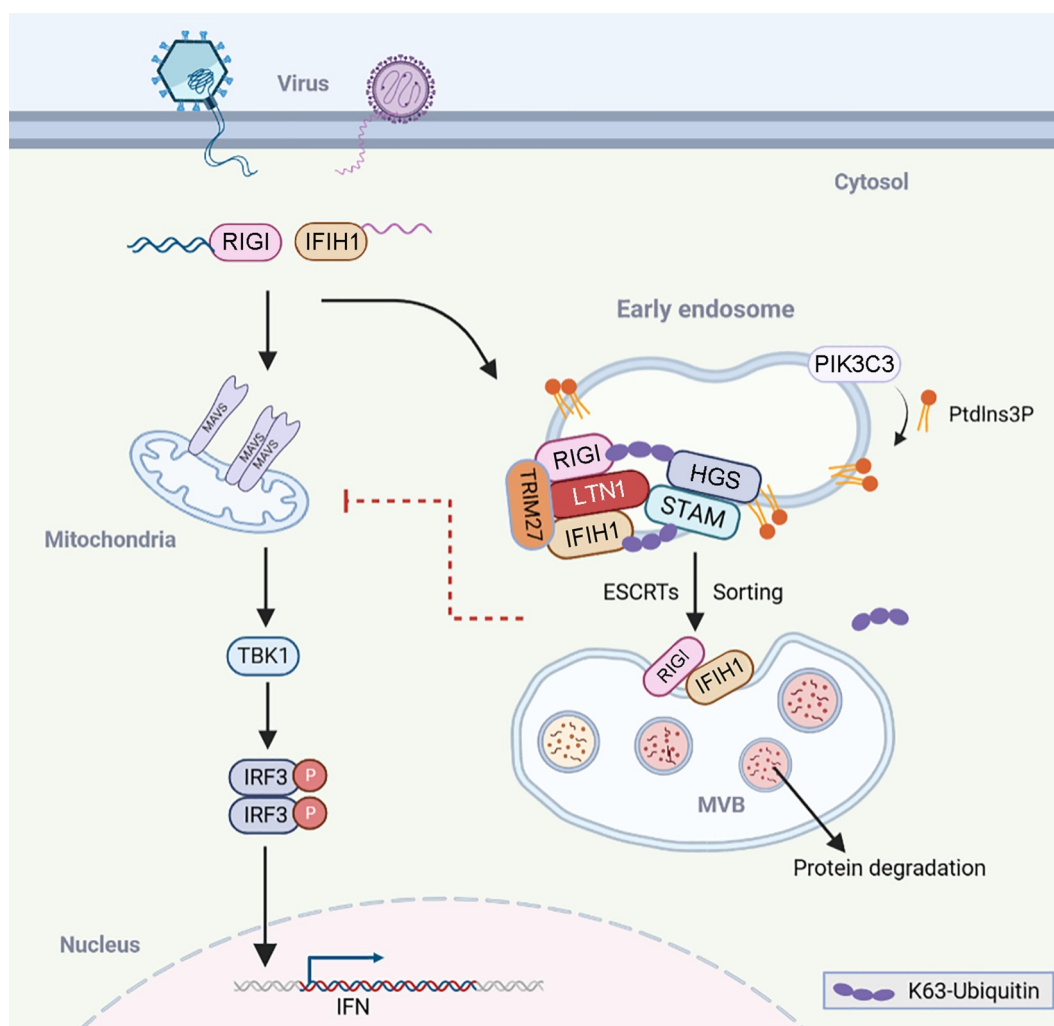


Figure 7. Working model to show LTN1 promotes endosomal degradation of RIGI and IFIH1 through ESCRT machinery. LTN1 promotes K63-linked polyubiquitination of RIGI and IFIH1 by recruiting TRIM27, which facilitates endosome sorting and degradation of RIGI and IFIH1 through the ESCRT complex. This figure was drawn using <https://biorender.com/>.

addition to its well-known function in ribosome-associated protein quality control. Our research also revealed a new mechanism for regulating RIGI and IFIH1 degradation through ESCRT pathway. Therefore, the regulation of RIGI and IFIH1 expression by LTN1 holds promise as an intervention for diseases characterized by abnormal activation of innate immune responses.

Materials and methods

Reagents and antibodies

The following reagents were used in this study: Phorbol 12-myristate 13-acetate (PMA) (Sigma, P1585); MG132 (Sigma, C2211); bafilomycin A₁ (Invitrogen, tlr-Baf1); 3-methyladenine (Sigma, M9281); wortmannin (Medchemexpress, HY-10197); poly(I:C) (Invitrogen, tlr-pic); cGAMP (Invitrogen, tlr-nacga23-1); 5'-pppRNA (Invitrogen, tlr-3prna); SAR405 (Medchemexpress, HY-12481); Flag-peptide (Sigma, F4799).

The following antibodies were used in this study: anti-LTN1 (Abcam, ab104375); anti-IRF3 (Cell Signaling Technology, 4302s); anti-VSVG (Sigma, v5507); anti-p-IRF3

(Cell Signaling Technology, 4947s); anti-TBK1 (Cell Signaling Technology, 3504s); anti-p-TBK1 (Cell Signaling Technology, 5483s); anti-RIGI (Cell Signaling Technology, 3743s); anti-IFIH1 (Cell Signaling Technology, 5321s); anti-MAVS (Santa Cruz Biotechnology, sc-365333); anti-ATG5 (Cell Signaling Technology, 12994s); anti-ATG7 (Cell Signaling Technology, 8558s); anti-His (Cell Signaling Technology, 12698S); anti-Flag (M2; Sigma, f1804); anti-DDDDK tag (Abcam, ab1257); anti-HGS (Santa cruz biotechnology, sc-71455); PIK3C3/PI3-kinase p100 (Santa Cruz Biotechnology, sc-365404); mouse anti-MYC (Origene, TA150121); goat-anti-mouse Alexa Fluor 568 (Invitrogen, A-11004); goat-anti-rabbit Alexa Fluor 488 (Invitrogen, A-11034); anti-TRIM27 (Proteintech 12205-1-p); anti-NEMF (Proteintech 11840-1-p); anti-SQSTM1/p62 (Abcam, ab240635), anti-TCF25 (Abcam, ab67762).

Animal studies

The *Ltn1*^{fl/fl} mice were generated by Beijing Biocytogen (Beijing, China) using the CRISPR-Cas9 system. Simply, construct a Cas9-sgRNA expression plasmid and a targeting

vector containing a loxP site. Then, insert the plasmid upstream and the targeting vector downstream of exons 3–5. Microinject the linearized Cas9-sgRNA and targeting vector into mouse zygotes and implant the injected zygotes into C57BL/6 female mice. Genotyping was performed by PCR using the following primers: forward 5'-CGTTGCTTTCGCCTTGGATCAGTTA-3', reverse 5'-ATTTAGCTTGTGTGCCTTTCGCTCT-3'. *Lyz2-Cre* mice were obtained from The Jackson Laboratory. The primers for *Lyz2-Cre* transgenic mice genotyping were oIMR3066 mutant 5'-CCCAGAAATGCCAGATTACG-3', oIMR3067 common 5'-CTTGGGCTGCCAGAATTTCTC-3', oIMR3068 Wild type 5'-TTACAGTCGCCAGGCTGAC-3'. *Ltn1^{fl/fl}* mice used in our experiments were Cre-negative littermates of the *Ltn1^{fl/fl}Lyz2-Cre* mice. All mice used were 6–8 weeks of age. Mice were housed in individually ventilated cages. All mice with C57BL/6 background were reared without specific pathogens, approved by the Scientific Investigation Board of the Medical School of Shandong University.

Elisa

ELISA kits (Biolegend 439,407) were used to detect the concentration of IFN β in culture supernatant and serum samples.

Viral infection and plaque assay

VSV and VSV-GFP virus were got from H. Meng (Institute of Basic Medicine, Shandong Academy of Medical Sciences, China) and SeV was purchased from China Center for Type Culture Collection (Wuhan University, China). HEK293T (National Collection Of Authenticated Cell Cultures), THP-1 (National Collection Of Authenticated Cell Cultures), BMDMs or primary peritoneal macrophages (4×10^5) were plated 24 h. After that, we added VSV (MOI = 0.1) or SeV to the cells at the prescribed time. As previously described, VSV plaque detection was performed in HEK293 cells [47].

Coimmunoprecipitation and immunoblot analysis

Cells were incubated in cell lysis buffer (Sigma, C2978) containing complete protease inhibitor (Sigma, S8820) for 30 min, and then centrifuged at 4°C for 10 min. For each immunoprecipitation assay, cells were lysed with IP buffer (1% [v:v] Nonidet P-40 [Solarbio, N8030], 50 mM Tris-HCl, pH 7.4, 50 mM EDTA, 150 mM NaCl and protease inhibitor mixture [Sigma, S8820]). Proteins were quantified by a Pierce™ BCA Protein Assay Kit according to the manufacturer's instruction (Thermo Scientific 23,225). The supernatant was mixed with 0.5 μ g incubate the indicator antibody of for 1 h, and then we added 35 μ l incubated protein A/G PLUS-Agarose (Santa Cruz Biotechnology, sc-2003) to the mixture overnight. Cell lysates or immunoprecipitates were separated by SDS-PAGE and western blotting analysis was performed.

CRISPR-Cas9 knockout

Genome engineering via the CRISPR-Cas9 system involved cloning double-stranded oligonucleotides that corresponded

to the target sequences into the lentiCRISPR V2 vector. The resulting construct was then co-transfected into HEK293T cells, which were subsequently selected with puromycin (3 μ g/mL) for at least 5 days starting 2 days after transfection. The pool of sorted cells was either directly used in subsequent functional assays or diluted into 96-well plates by serial dilutions to obtain single clones. The knockout efficiency was examined by RT-qPCR analysis or immunoblotting analysis.

RNA knockdown

For siRNA knockdown, THP-1 or macrophages were planted in 6- or 24-well plates, and the siRNA oligomers were transfected using the Lipofectamine™ RNAiMAX Transfection Reagent (Invitrogen 13,778,150) according to the recommendation of the manufacturer. siRNA (final concentration, 100 nM) reagents were transfected into each well. The knockdown efficiency was detected by quantitative real-time PCR after 48 h transfection, or continued to the subsequently indicated treatment.

mRNA isolation and real-time PCR

Cells were collected and the total RNA was extracted from whole cell lysates using an EASYspin Plus tissue/cell rapid RNA extraction kit (Aidlab, RN2802) and the diluted RNA of total RNA was reverse transcribed with a PrimeScript™ RT reagent Kit (Takara, R047A). The SYBR RT-PCR kit (Roche 06,924,204,001) was used for quantitative real-time PCR (qPCR) analysis in triplicate wells. The analysis was conducted with an iCycler IQ thermal cycler and detection system (Bio-Rad) following the manufacturer's instructions. The *ACTB* housekeeping gene in each individual sample was used for normalization. The $2^{-\Delta\Delta C_t}$ method was used to calculate relative expression changes. Detailed primers are listed in Table S1.

Confocal microscopy

After transfecting HEK293T cells with the relevant expression plasmid, the cells were fixed with 4% paraformaldehyde for 15 min and permeabilized with 0.05% Triton X-100 (Beyotime, P0096) in PBS (Solarbio, P1020) for 15 min. The cells were then blocked for 1 h with 2% BSA (Geneview, 9048-46-8), incubated overnight at 4°C with the primary antibody, and subsequently incubated with the secondary antibody (1:1000). LSM 880 Meta confocal microscope (Carl Zeiss, Jena, Germany) was employed to capture images of the cells.

Confocal time-lapse imaging

HEK293T Cells were planted in 0.17 ± 0.005 mm glass bottom dishes (Cellvis) overnight and transfected with GFP-mCherry-RIGI (this paper) or GFP-mCherry-IFIH1 (this paper) for 12 h, followed by transfection with Flag-LTN1 (this paper) for 12 h and the images were got using an Opera Phenix High-Content Screening System (Perkin Elmer, USA). During imaging, cells were sustained in a heated incubation incubator at

37°C with CO₂. Morphologic analysis was implemented using with Harmony Software (V4.9, Perkin Elmer).

Virus infection in vivo

Littermate mice of wild type and *Itih1^{fl/fl}Lyz2-Cre* mice were distributed into groups according to age and sex and then were given intravenous (i.v.) injection with VSV (1×10^8 PFU per mouse) or intraperitoneal injection with VSV (5×10^7 PFU per mouse). The concentration of IFNB was detected by ELISA. The VSV titers in the spleen, lung or liver were detected by standard plaque assays. The survival rate of mice infected with VSV was evaluated by survival test. We separated mouse lungs, fixed them in 10% phosphate buffered formalin, then cultured into paraffin sections, stained with hematoxylin eosin, and examined histological changes under light microscopy.

Protein purification

A TNT Quick Coupled Transcription/Translation System kit (Promega, L1171) was used to express *IFIH1*, *RIGI*, *TRIM27* gene or *TRIM27* (C/A) gene according to the method provided by the manufacturer. *IFIH1* in the pcDNA6B-Flag expression vector was a kind gift from Dr. Peihui Wang (Shandong University, China) as described previously [48]. Flag-LTN1, Flag-LTN1 (Δ HEAT) and Flag-LTN1 (Δ R) proteins were purified in HEK293T cells using anti-FLAG M2 affinity gel (Sigma, A2220) and 3 \times FLAG peptide (Sigma, F4799). Briefly, Flag-tagged vectors were expressed in HEK293T cells by Lipofectamine 3000 reagents (Invitrogen, L3000015). After 48 h of transfection, cells were lysed in the IP Buffer (1% NP-40 [solarbio, N8030], 50 mM Tris-HCl pH 7.4, 50 mM EDTA, 150 mM NaCl and protease inhibitors). After centrifugation at 12,000 g for 10 min, Flag- was captured on anti-Flag agarose beads (Millipore, A2220) and eluted using the Flag peptide.

Stimulants transfection

HMW Poly(I:C) (Invitrogen, tlr1-pic) and 5'-pppRNA (Invitrogen, tlr1-3prna) were purchased from Invitrogen. Stimulants were used at the following concentrations: 5'-pppRNA, 0.5 μ g ml⁻¹; HMW poly(I:C), 1 μ g ml⁻¹. For transfection, stimulants were transfected in cells using Lipofectamine 2000 reagents (Invitrogen 11,668,019).

In vitro ubiquitination assay

The in vitro ubiquitination assays were conducted according to previously described methods [47]. Recombinant Human Ubiquitin Protein (Boston Biochem, U-100 H-10 M), UBE1 (Boston Biochem, E-306-050), and UBE2D1/UbcH5a Protein (Boston Biochem, E2-616-100) were applied to analyze ubiquitination according to the protocol recommended by the manufacturer. Briefly, UBA1, UBE2D1, LTN1, TRIM27 or TRIM27 (C/A) and RIGI or IFIH1 proteins were mixed with

reaction buffer, ubiquitin, ATP and MgCl₂. The reaction mix was incubated at 30°C for 1 h, followed by added with 6 \times SDS loading buffer at 98°C for 8 min to stop the reaction.

Statistical analysis

All data were obtained from at least three independent experiments and the results are comparable. Data processing was based on GraphPad Prism7.0, and is carried out by unpaired t-test. All data were showed as mean \pm S.D. of one representative experiment. In the animal survival test, the Kaplan-Meier survival curve was drawn and analyzed by the log-rank method. * $P < 0.05$ was considered statistically significant.

Ethics statement

All animal experiments were undertaken in accordance with the National Institute of Health Guide for the Care and Use of Laboratory Animals, with the approval of the Ethics Committee of Scientific Research of Shandong University Qilu Hospital, Jinan, Shandong Province, China (Permit number: KYLL-2017[KS]-361).

Acknowledgements

We would like to kindly thank many colleagues who provided key reagents used in our experiment. We also thank the technical support for confocal microscopy analysis from M.L. Wu and Y. Yu in the Translational Medicine Core Facility of Advanced Medical Research Institute, Shandong University.

Disclosure statement

No potential conflict of interest was reported by the author(s).

Funding

This work was supported by grants from the National Natural Science Foundation of China (82321002, 32230033, 81930039 to C.G., and 82222027, 32270918, 31900680 to B.L.). This work was also supported by the National Key Research and Development Program of China (2021YFC2300603 to C.G.) and the Shandong Provincial Natural Science Foundation (ZR2021YQ48, ZR2018BC021, ZR2021ZD08 to B. L.).

Data availability statement

Data in support of the findings of this study are available from the corresponding author upon request.

References

- [1] Hu B, Guo H, Zhou P, et al. Characteristics of SARS-CoV-2 and COVID-19. *Nat Rev Microbiol.* 2021;19(3):141–154. doi: [10.1038/s41579-020-00459-7](https://doi.org/10.1038/s41579-020-00459-7)
- [2] Wang T, Zhang J, Wang Y, et al. Influenza-trained mucosal-resident alveolar macrophages confer long-term antimicrobial immunity in the lungs. *Nat Immunol.* 2023;24(3):423–438. doi: [10.1038/s41590-023-01428-x](https://doi.org/10.1038/s41590-023-01428-x)
- [3] Wong LR, Perlman S. Immune dysregulation and immunopathology induced by SARS-CoV-2 and related coronaviruses - are we our own

- worst enemy? *Nat Rev Immunol.* 2022;22(1):47–56. doi: [10.1038/s41577-021-00656-2](https://doi.org/10.1038/s41577-021-00656-2)
- [4] Tregoning JS, Flight KE, Higham SL, et al. Progress of the COVID-19 vaccine effort: viruses, vaccines and variants versus efficacy, effectiveness and escape. *Nat Rev Immunol.* 2021;21(10):626–636. doi: [10.1038/s41577-021-00592-1](https://doi.org/10.1038/s41577-021-00592-1)
- [5] Akira S, Uematsu S, Takeuchi O. Pathogen recognition and innate immunity. *Cell.* 2006;124(4):783–801. doi: [10.1016/j.cell.2006.02.015](https://doi.org/10.1016/j.cell.2006.02.015)
- [6] Brubaker SW, Bonham KS, Zanoni I, et al. Innate immune pattern recognition: a cell biological perspective. *Annu Rev Immunol.* 2015;33(1):257–290. doi: [10.1146/annurev-immunol-032414-112240](https://doi.org/10.1146/annurev-immunol-032414-112240)
- [7] Ablasser A, Hur S. Regulation of cGAS- and RLR-mediated immunity to nucleic acids. *Nat Immunol.* 2020;21(1):17–29. doi: [10.1038/s41590-019-0556-1](https://doi.org/10.1038/s41590-019-0556-1)
- [8] Coccia EM, Battistini A. Early IFN type I response: learning from microbial evasion strategies. *Semin Immunol.* 2015;27(2):85–101. doi: [10.1016/j.smim.2015.03.005](https://doi.org/10.1016/j.smim.2015.03.005)
- [9] Fernandez-Ruiz R, Niewold TB. Type I interferons in autoimmunity. *J Invest Dermatol.* 2022;142(3 Pt B):793–803. doi: [10.1016/j.jid.2021.11.031](https://doi.org/10.1016/j.jid.2021.11.031)
- [10] Raiborg C, Stenmark H. The ESCRT machinery in endosomal sorting of ubiquitylated membrane proteins. *Nature.* 2009;458(7237):445–452. doi: [10.1038/nature07961](https://doi.org/10.1038/nature07961)
- [11] Henne WM, Buchkovich NJ, Emr SD. The ESCRT pathway. *Dev Cell.* 2011;21(1):77–91. doi: [10.1016/j.devcel.2011.05.015](https://doi.org/10.1016/j.devcel.2011.05.015)
- [12] Ren X, Kloer DP, Kim YC, et al. Hybrid structural model of the complete human ESCRT-0 complex. *Structure.* 2009;17(3):406–416. doi: [10.1016/j.str.2009.01.012](https://doi.org/10.1016/j.str.2009.01.012)
- [13] Flower TG, Takahashi Y, Hudait A, et al. A helical assembly of human ESCRT-I scaffolds reverse-topology membrane scission. *Nat Struct Mol Biol.* 2020;27(6):570–580. doi: [10.1038/s41594-020-0426-4](https://doi.org/10.1038/s41594-020-0426-4)
- [14] Hierro A, Sun J, Rusnak AS, et al. Structure of the ESCRT-II endosomal trafficking complex. *Nature.* 2004;431(7005):221–225. doi: [10.1038/nature02914](https://doi.org/10.1038/nature02914)
- [15] Teis D, Saksena S, Emr SD. Ordered assembly of the ESCRT-III complex on endosomes is required to sequester cargo during MVB formation. *Dev Cell.* 2008;15(4):578–589. doi: [10.1016/j.devcel.2008.08.013](https://doi.org/10.1016/j.devcel.2008.08.013)
- [16] Babst M, Wendland B, Estepa EJ, et al. The Vps4p AAA ATPase regulates membrane association of a vps protein complex required for normal endosome function. *EMBO J.* 1998;17:2982–2993. doi: [10.1093/emboj/17.11.2982](https://doi.org/10.1093/emboj/17.11.2982)
- [17] Kuchitsu Y, Mukai K, Uematsu R, et al. STING signalling is terminated through ESCRT-dependent microautophagy of vesicles originating from recycling endosomes. *Nat Cell Biol.* 2023;25(3):453–466. doi: [10.1038/s41556-023-01098-9](https://doi.org/10.1038/s41556-023-01098-9)
- [18] Gentili M, Liu B, Papanastasiou M, et al. ESCRT-dependent STING degradation inhibits steady-state and cGAMP-induced signalling. *Nat Commun.* 2023;14(1):611. doi: [10.1038/s41467-023-36132-9](https://doi.org/10.1038/s41467-023-36132-9)
- [19] Wang X, Rimal S, Tantray I, et al. Prevention of ribosome collision-induced neuromuscular degeneration by SARS CoV-2-encoded Nsp1. *Proc Natl Acad Sci U S A.* 2022;119(42):e2202322119. doi: [10.1073/pnas.2202322119](https://doi.org/10.1073/pnas.2202322119)
- [20] Lyumkis D, Oliveira dos Passos D, Tahara EB, et al. Structural basis for translational surveillance by the large ribosomal subunit-associated protein quality control complex. *Proc Natl Acad Sci U S A.* 2014;111(45):15981–15986. doi: [10.1073/pnas.1413882111](https://doi.org/10.1073/pnas.1413882111)
- [21] Doamekpor SK, Lee JW, Hepowit NL, et al. Structure and function of the yeast listerin (Ltn1) conserved N-terminal domain in binding to stalled 60S ribosomal subunits. *Proc Natl Acad Sci U S A.* 2016;113(29):E4151–4160. doi: [10.1073/pnas.1605951113](https://doi.org/10.1073/pnas.1605951113)
- [22] Vietri M, Radulovic M, Stenmark H. The many functions of ESCRTs. *Nat Rev Mol Cell Biol.* 2020;21(1):25–42. doi: [10.1038/s41580-019-0177-4](https://doi.org/10.1038/s41580-019-0177-4)
- [23] Hurley JH, Hanson PI. Membrane budding and scission by the ESCRT machinery: it's all in the neck. *Nat Rev Mol Cell Biol.* 2010;11(8):556–566. doi: [10.1038/nrm2937](https://doi.org/10.1038/nrm2937)
- [24] Bengtson MH, Joazeiro CA. Role of a ribosome-associated E3 ubiquitin ligase in protein quality control. *Nature.* 2010;467(7314):470–473. doi: [10.1038/nature09371](https://doi.org/10.1038/nature09371)
- [25] Lauwers E, Jacob C, André B. K63-linked ubiquitin chains as a specific signal for protein sorting into the multivesicular body pathway. *J Cell Bio.* 2009;185(3):493–502. doi: [10.1083/jcb.200810114](https://doi.org/10.1083/jcb.200810114)
- [26] Li WW, Nie Y, Yang Y, et al. Ubiquitination of TLR3 by TRIM3 signals its ESCRT-mediated trafficking to the endolysosomes for innate antiviral response. *Proc Natl Acad Sci U S A.* 2020;117(38):23707–23716. doi: [10.1073/pnas.2002472117](https://doi.org/10.1073/pnas.2002472117)
- [27] Hao YH, Doyle JM, Ramanathan S, et al. Regulation of WASH-dependent actin polymerization and protein trafficking by ubiquitination. *Cell.* 2013;152(5):1051–1064. doi: [10.1016/j.cell.2013.01.051](https://doi.org/10.1016/j.cell.2013.01.051)
- [28] Wang J, Zhao D, Lei Z, et al. TRIM27 maintains gut homeostasis by promoting intestinal stem cell self-renewal. *Cell Mol Immunol.* 2023;20(2):158–174. doi: [10.1038/s41423-022-00963-1](https://doi.org/10.1038/s41423-022-00963-1)
- [29] Harhaj E, Zurek B, Schoultz I, et al. TRIM27 negatively regulates NOD2 by ubiquitination and proteasomal degradation. *PLoS One.* 2012;7(7):e41255. doi: [10.1371/journal.pone.0041255](https://doi.org/10.1371/journal.pone.0041255)
- [30] Sundaramoorthy E, Ryan AP, Fulzele A, et al. Ribosome quality control activity potentiates vaccinia virus protein synthesis during infection. *J Cell Sci.* 2021;134(8). doi: [10.1242/jcs.257188](https://doi.org/10.1242/jcs.257188)
- [31] Wang G, Kouwaki T, Okamoto M, et al. Attenuation of the innate immune response against viral infection due to ZNF598-promoted binding of FAT10 to RIG-I. *Cell Rep.* 2019;28(8):1961–1970 e1964. doi: [10.1016/j.celrep.2019.07.081](https://doi.org/10.1016/j.celrep.2019.07.081)
- [32] Joazeiro CAP. Mechanisms and functions of ribosome-associated protein quality control. *Nat Rev Mol Cell Biol.* 2019;20(6):368–383. doi: [10.1038/s41580-019-0118-2](https://doi.org/10.1038/s41580-019-0118-2)
- [33] Wan L, Juszkievicz S, Blears D, et al. Translation stress and collided ribosomes are co-activators of cGAS. *Mol Cell.* 2021;81(13):2808–2822 e2810. doi: [10.1016/j.molcel.2021.05.018](https://doi.org/10.1016/j.molcel.2021.05.018)
- [34] Batool M, Kim MS, Choi S. Structural insights into the distinctive RNA recognition and therapeutic potentials of RIG-I-like receptors. *Med Res Rev.* 2022;42(1):399–425. doi: [10.1002/med.21845](https://doi.org/10.1002/med.21845)
- [35] Rehwinkel J, Gack MU. RIG-I-like receptors: their regulation and roles in RNA sensing. *Nat Rev Immunol.* 2020;20(9):537–551. doi: [10.1038/s41577-020-0288-3](https://doi.org/10.1038/s41577-020-0288-3)
- [36] Nejentsev S, Walker N, Riches D, et al. Rare variants of IFIH1, a gene implicated in antiviral responses, protect against type 1 diabetes. *Science.* 2009;324(5925):387–389. doi: [10.1126/science.1167728](https://doi.org/10.1126/science.1167728)
- [37] Van Eyck L, De Somer L, Pombal D, et al. Brief report: IFIH1 Mutation Causes systemic lupus erythematosus with selective IgA deficiency. *Arthritis & Rheumat.* 2015;67(6):1592–1597. doi: [10.1002/art.39110](https://doi.org/10.1002/art.39110)
- [38] Strange A, Capon F, Spencer CC, et al. A genome-wide association study identifies new psoriasis susceptibility loci and an interaction between HLA-C and ERAP1. *Nat Genet.* 2010;42(11):985–990.
- [39] Ahmad S, Mu X, Yang F, et al. Breaching self-tolerance to alu duplex RNA underlies MDA5-mediated inflammation. *Cell.* 2018;172(4):797–810.e713. doi: [10.1016/j.cell.2017.12.016](https://doi.org/10.1016/j.cell.2017.12.016)
- [40] Arimoto K, Takahashi H, Hishiki T, et al. Negative regulation of the RIG-I signaling by the ubiquitin ligase RNF125. *Proc Natl Acad Sci U S A.* 2007;104(18):7500–7505. doi: [10.1073/pnas.0611551104](https://doi.org/10.1073/pnas.0611551104)

- [41] Sun R, Guo Y, Li X, et al. PRRSV non-Structural proteins orchestrate porcine E3 ubiquitin ligase RNF122 to promote PRRSV proliferation. *Viruses*. 2022;14(2):424. doi: [10.3390/v14020424](https://doi.org/10.3390/v14020424)
- [42] Zhao C, Jia M, Song H, et al. The E3 ubiquitin ligase TRIM40 attenuates antiviral immune responses by targeting MDA5 and RIG-I. *Cell Rep*. 2017;21(6):1613–1623. doi: [10.1016/j.celrep.2017.10.020](https://doi.org/10.1016/j.celrep.2017.10.020)
- [43] Hou P, Yang K, Jia P, et al. A novel selective autophagy receptor, CCDC50, delivers K63 polyubiquitination-activated RIG-I/MDA5 for degradation during viral infection. *Cell Res*. 2021;31(1):62–79. doi: [10.1038/s41422-020-0362-1](https://doi.org/10.1038/s41422-020-0362-1)
- [44] Du Y, Duan T, Feng Y, et al. LRRC25 inhibits type I IFN signaling by targeting ISG15-associated RIG-I for autophagic degradation. *EMBO J*. 2018;37(3):351–366. doi: [10.15252/embj.201796781](https://doi.org/10.15252/embj.201796781)
- [45] Joazeiro CAP. Ribosomal stalling during translation: providing substrates for ribosome-associated protein quality control. *Annu Rev Cell Dev Biol*. 2017;33(1):343–368. doi: [10.1146/annurev-cellbio-111315-125249](https://doi.org/10.1146/annurev-cellbio-111315-125249)
- [46] Zheng Q, Hou J, Zhou Y, et al. Siglec1 suppresses antiviral innate immune response by inducing TBK1 degradation via the ubiquitin ligase TRIM27. *Cell Res*. 2015;25(10):1121–1136. doi: [10.1038/cr.2015.108](https://doi.org/10.1038/cr.2015.108)
- [47] Liu B, Zhang M, Chu H, et al. The ubiquitin E3 ligase TRIM31 promotes aggregation and activation of the signaling adaptor MAVS through Lys63-linked polyubiquitination. *Nat Immunol*. 2017;18(2):214–224. doi: [10.1038/ni.3641](https://doi.org/10.1038/ni.3641)
- [48] Zheng Y, Zhuang MW, Han L, et al. Severe acute respiratory syndrome coronavirus 2 (SARS-CoV-2) membrane (M) protein inhibits type I and III interferon production by targeting RIG-I/MDA-5 signaling. *Signal Transduct Target Ther*. 2020;5(1):299. doi: [10.1038/s41392-020-00438-7](https://doi.org/10.1038/s41392-020-00438-7)